Article: 58166 / Vol. 595 No. 1 / Printed: Tuesday 15th July 2003 /

THE ASTROPHYSICAL JOURNAL, 595:000–000, 2003 September 20
© 2003. The American Astronomical Society. All rights reserved. Printed in U.S.A.

OBSERVATIONS OF ROTATIONALLY RESOLVED C_3 IN TRANSLUCENT SIGHT LINES

MÁTÉ ÁDÁMKOVICS,[1] GEOFFREY A. BLAKE,[2] AND BENJAMIN J. MCCALL[1,3]

Received 2003 April 30; accepted 2003 June 3

ABSTRACT

The rotationally resolved spectrum of the $A^1\Pi_u \leftarrow X^1\Sigma_g^+$ 000–000 transition of C_3, centered at 4051.6 Å, has been observed along 10 translucent lines of sight. To interpret these spectra, a new method for the determination of column densities and analysis of excitation profiles involving the simulation and fitting of observed spectra has been developed. The populations of lower rotational levels ($J \leq 14$) in C_3 are best fitted by thermal distributions that are consistent with the kinetic temperatures determined from the excitation profile of C_2. Just as in the case of C_2, higher rotational levels ($J > 14$) of C_3 show increased nonthermal population distributions in clouds that have been determined to have total gas densities below $\sim 500\ \mathrm{cm}^{-3}$.

Subject headings: astrochemistry — ISM: lines and bands — ISM: molecules

1. INTRODUCTION

The existence of carbon chain molecules in diffuse interstellar clouds raises questions about the chemistry that occurs in these clouds, as well as the fate of large carbonaceous molecules produced throughout the life cycles of stars. Carbon chain molecules have been suggested as the source of the confounding diffuse interstellar bands (DIBs; Douglas 1977); however, efforts to identify a specific molecular carrier have thus far failed. C_7^- and l-$C_3H_2^-$ have been the most recently rejected (McCall et al. 2001, 2002a) in a long list of candidates (Herbig 1995). The smallest carbon chain molecule, C_2, has been used as a powerful probe of the temperature and density in diffuse clouds (van Dishoeck & Black 1989), and, until very recently, diffuse cloud chemistry was understood only in terms of atoms and diatomics.

After repeated efforts (Clegg & Lambert 1982; Snow et al. 1988; Haffner & Meyer 1995), the first clear detections of C_3 in three diffuse clouds were reported by Maier et al. (2001). Since this first observational study of C_3 in the diffuse interstellar medium (ISM), a detailed model has been developed to understand its excitation (Roueff et al. 2002), and a low-resolution survey has detected it in 15 translucent sight lines (Oka et al. 2003). Along with infrared measurements of H_3^+ (McCall et al. 1998, 2002b; Geballe et al. 1999), which can directly probe the interstellar cosmic-ray ionization rate (McCall et al. 2003b), the detections of C_3 demonstrate that the chemistry of diffuse clouds may be significantly richer than expected.

The "λ4050 group" of C_3 was first observed in emission in comet Tebutt (Huggins 1881) and has since been observed in the photospheres of many cool stars (Jørgensen 1994), in a few proto–planetary nebulae (Hrivnak & Kwok 1999), and toward many other comets (see, for example, recent work by Rousselot et al. 2001). The λ4050 group was first observed in the laboratory by Raffety (1916) in emission from the flame of a Mecker burner. Douglas (1951) identified the carrier of the group as C_3, and a detailed assignment as $A^1\Pi_u \leftarrow X^1\Sigma_g^+$ was made by Gausset et al. (1965). At longer wavelengths, C_3 has also been observed in the material around the asymptotic giant branch star IRC +10216 using both the asymmetric vibrational stretching mode at 4.9 μm (Hinkle et al. 1988) and the anomalously low-frequency bending mode at 157 μm (Cernicharo et al. 2000).

As a linear carbon chain, like C_2, C_3 has no permanent dipole moment and thus lacks the ability to cool efficiently via rotational transitions. High rotational levels of C_3, once produced during chemical formation or following UV pumping, can only relax slowly by collisional de-excitation and have significant lifetimes under interstellar conditions. Maier et al. (2001) reported that the low-J levels ($J < 14$) in their spectra of C_3 toward ζ Oph were fitted by a Boltzmann distribution at $T_l = 60$ K, whereas $J > 14$ were fitted by a Boltzmann distribution at $T_h = 230$ K.

Depending on the intensity of the UV radiation field, the rates of collisional (de-)excitation and UV pumping, and the photochemical lifetime of C_3, Roueff et al. (2002) suggest that the high rotational levels of C_3 may retain information about the temperature at which C_3 was formed, as well as the temperature and density of the cloud. Roueff et al. (2002) applied their sophisticated C_3 excitation model to all three of the detections by Maier et al. (2001)—ζ Oph, ζ Per, and 20 Aql—along with their own observations of HD 210121, but none of the observations determined the population of C_3 in $J > 14$ well enough to constrain the full excitation model. Galazutdinov et al. (2002) have since provided spectra of C_3 toward χ Oph and HD 152236, without analysis of the excitation.

With the guidance of the low-resolution survey results of Oka et al. (2003), we have measured the spectra of 24 reddened stars at high resolution in order to study the excitation profile of C_3 in a large sample of diffuse clouds. Here we present the rotationally resolved spectra of C_3 at high signal-to-noise ratio (S/N) in 10 of these translucent sight lines. We present a new spectral fitting method for determining the populations in each J level and examine the relationship between the rotational excitation of C_3 and C_2.

2. OBSERVATIONS

Observations were carried out using the Shane 3 m telescope and the Hamilton Echelle Spectrograph (Vogt 1987) at Lick Observatory on 2002 July 12 through 14 and using the High Resolution Echelle Spectrometer (HIRES; Vogt

[1] Department of Chemistry, University of California, Berkeley, CA 94720; mate@haze.cchem.berkeley.edu.

[2] Division of Geological and Planetary Sciences and Division of Chemistry and Chemical Engineering, M/S 150-21, California Institute of Technology, Pasadena, CA 91125.

[3] Astronomy Department, 601 Campbell Hall, University of California, Berkeley, CA 94720.

TABLE 1
DATA FOR PROGRAM STARS

Star	Name	Type	V	$E(B-V)$	D (pc)[a]	S/N[b]	Date (UT)
HD 11415	ϵ Cas	B3 III	3.38	0.05	136	2400	2002 Dec 15
HD 20041	...	A0 Ia	5.79	0.72	440	1000	2002 Dec 14
HD 21389	...	A0 Iae	4.54	0.57	940	1300	2002 Dec 14
HD 21483	...	B3 III	7.06	0.56	440	1000	2002 Dec 15
HD 22951	40 Per	B0.5 V	4.97	0.27	283	1700	2002 Dec 15
HD 23180	o Per	B1 III	3.83	0.31	280	1850	2002 Dec 14
HD 24398	ζ Per	B1 Ib	2.85	0.31	301	2200	2002 Dec 15
HD 24534	X Per	O9.5pe	6.10	0.59	590	1200	2002 Dec 15
HD 24912	ξ Per	O7e	4.04	0.33	470	2600	2002 Dec 14
HD 34078	AE Aur	O9.5 Ve	5.96	0.52	620	1200	2002 Dec 14
HD 35149	23 Ori	B1 V	5.00	0.11	450	2100	2002 Dec 15
HD 36371	χ Aur	B5I ab	4.76	0.43	880	2000	2002 Dec 15
HD 37022	θ^1 Ori C	O6	5.13	0.34	450	2000	2002 Dec 15
HD 37061	...	B1 V	6.83	0.52	580	1300	2002 Dec 15
HD 41117	χ^2 Ori	B2 Iae	4.63	0.45	1000	2100	2002 Dec 15
HD 42087	3 Gem	B.25 Ibe	5.75	0.36	1200	1600	2002 Dec 14
HD 43384	9 Gem	B3 Ib	6.25	0.58	1100	1600	2002 Dec 14
HD 53367	...	B0 IVe	6.96	0.74	780	1300	2002 Dec 15
HD 62542	...	B5 V	8.04	0.35	246	700	2002 Dec 14
HD 169454	...	B1.5 Ia	6.61	1.12	930	450	2002 Jul 14
HD 204827	...	B0 V	7.94	1.11	600	650	2002 Dec 14, 2002 Jul 13
HD 206267	...	O6 f	5.62	0.53	1000	1200	2002 Jul 12, 2002 Jul 13
HD 207198	...	O9 IIe	5.95	0.62	1000	700	2002 Jul 12, 2002 Jul 13
HD 210839	λ Cep	O6 If	5.04	0.57	505	700	2002 Jul 13

[a] The distance to θ^1 Ori C is from Shuping & Snow 1997. All other distances are taken from Thorburn et al. 2003 and Oka et al. 2003.
[b] Signal to noise per pixel, measured near 4049 Å.

et al. 1994) on the 10 m Keck I telescope atop Mauna Kea on 2002 December 14 and 15.

The Hamilton spectrograph operates with an echelle grating and two cross-dispersing prisms, is mounted at coudé focus, and provides nearly complete spectral coverage from 3500 to 10000 Å. The detector used was the Lick3 L4-9-00AR thinned 2048×2048 CCD with 15 μm pixels. The $1''.2$ wide and $2''.0$ long slit provides a resolving power $R = \lambda/\Delta\lambda \sim 60,000$, where the resolution $\Delta\lambda$ refers to the FWHM of the instrument profile, ~0.1 Å at 6000 Å, which spans 2 pixels on the detector. The reduced data have a dispersion $d = 0.0336$ Å pixel^{-1} at 4050 Å.

The HIRES instrument is also a cross-dispersed echelle spectrograph and features a backside-illuminated Tek 2048×2048 CCD detector functioning over the 3500–10000 Å range and capturing a spectral span of 1200–2500 Å per exposure. To minimize total readout time for our relatively bright targets, high gain mode and dual-amp readout were used. For these observations, spectra in the 3985–6420 Å range were recorded with each exposure, with small gaps in the spectral coverage starting at ~5000 Å and increasing to ~30 Å at 6315 Å, owing to echelle orders falling off the edge of the CCD. A slit size of $0''.574 \times 14''$ was used to achieve a resolving power of $R \sim 67,000$. The detector position was constant throughout each night and moved only slightly between the two nights of observations. The reduced data have a dispersion $d = 0.0287$ Å pixel^{-1} at 4050 Å.

The data were reduced using standard procedures in the echelle package in NOAO's Image Reduction and Analysis Facility (IRAF). As many as 120 flat-field images were taken before and 180 after the observations to ensure that the S/N of the reduced spectra was photon-counting limited. Calibration and target images were bias-corrected and combined, before target images were flat-fielded and echelle apertures extracted. Wavelength calibration was performed with standard routines using spectra of a ThAr lamp, and one-dimensional spectra of the targets were extracted for further analysis. Generally, the entire aperture blaze was fitted with a low-order polynomial to normalize the spectra. In cases where the spectral features of interest were observed very close to the center (maximum) of the aperture blaze, only a small spectral region around the features was continuum fitted with a low-order polynomial. The program stars and their properties, along with the S/N achieved at 4049 Å, are shown in Table 1. Figure 1 presents the C_3 spectra observed along the 10 lines of sight with detectable C_3 absorption.

3. SPECTRUM OF C_3

Unlike molecules that can radiate away excess energy, the distribution of population among rotational levels for molecules in the ISM without a permanent dipole moment, such as C_3, is a delicate balance between collisional and radiative processes. This has been studied in detail for the homonuclear diatomics H_2 (Black & Dalgarno 1977 and references therein) and C_2 (van Dishoeck & Black 1982), and more recently a similar method of analysis has been used to examine C_3 (Roueff et al. 2002). In general, these models show that the populations of lower rotational levels ($J \lesssim 14$ for C_3) are controlled mostly by the kinetic temperature of the gas along the line of sight, whereas the populations in higher rotational levels are determined by the competition between

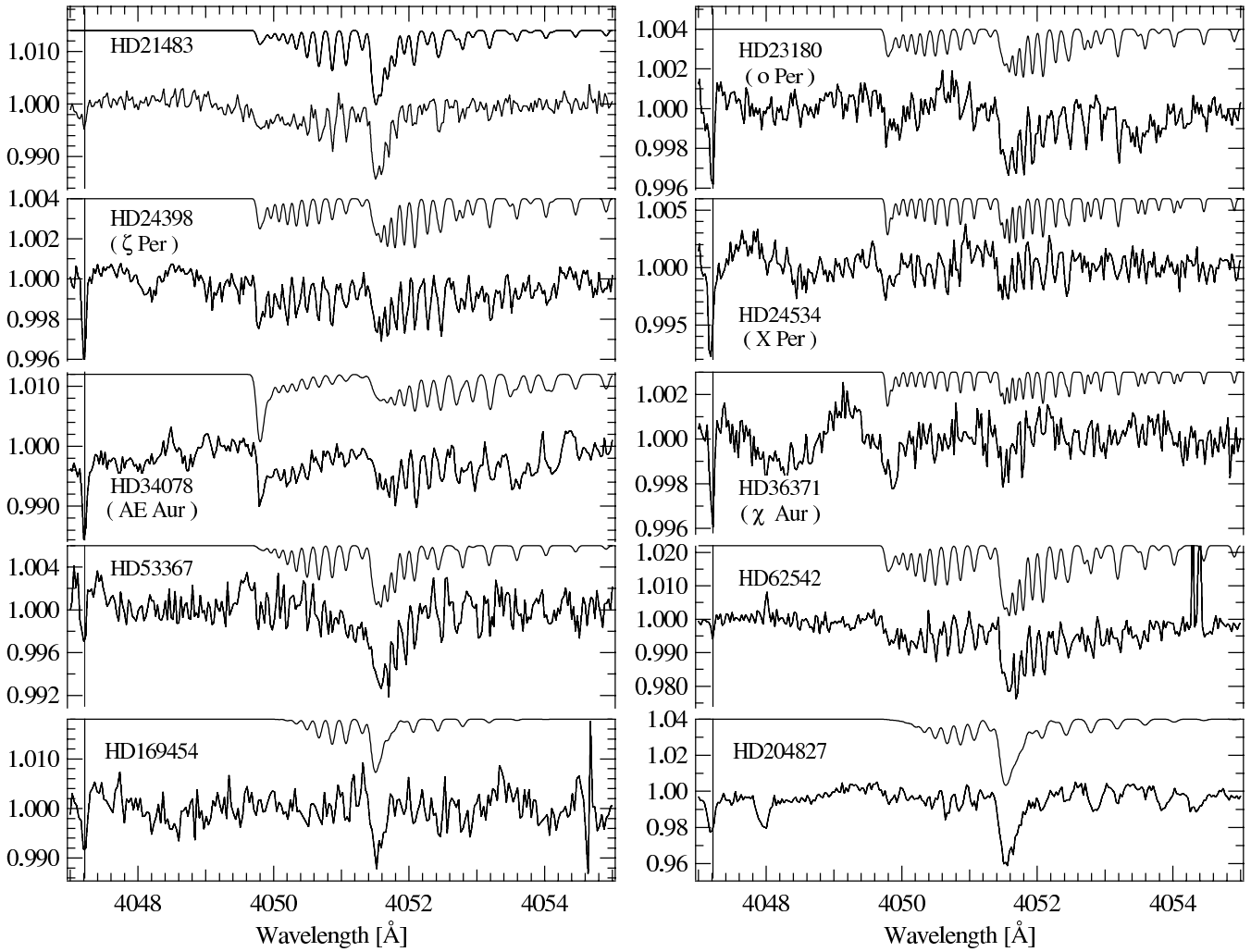

FIG. 1.—Spectra of translucent sight lines toward which C_3 was detected, along with thermal excitation model fits. Note how the Q-branch at 4051.6 Å is very well fitted, while the R band head at 4049.8 Å is sometimes underestimated. Spectra are all shifted to rest wavelengths, and the K I line at 4047.2 Å is marked by a vertical line. Broad stellar lines have been removed from the spectra of ζ Per, HD 21483, AE Aur, HD 36371, and HD 53367 using Gaussian line profiles.

radiative pumping and collisional de-excitation. The net result can be a nonthermal enhancement of high-J populations in low-density environments as observed by Maier et al. (2001) toward ζ Oph.

In order to determine the total column density of C_3 and measure the population distribution among rotational levels, we have used two models to fit 40 rovibronic transitions between 4049 and 4055 Å. A thermal excitation model incorporating either one or two temperatures was used, as well as a model that fit the population in each rotational level to the observed spectra. These two methods provided a means to extract information from overlapping or unresolved transitions in the C_3 Q-branch and R-branch band head.

Laboratory measurements (Gausset et al. 1965) of transition wavelengths were used in both models, with the exception of a shifted $R(0)$ line that was used in the rotational level population model (see § 3.4).

3.1. *Thermal Excitation Model*

In this model the relative population of each rotational level ($J \leq 30$) is determined using a thermal distribution at temperature, T. The fraction of total molecules in a particular J level is given by

$$F_J(T) = \frac{2J+1}{q_r} \exp\left[\frac{-hcB_0}{kT} J(J+1)\right] , \qquad (1)$$

where q_r is the rotational partition function given by

$$q_r = \sum_{J\,\mathrm{even}}^{\infty} (2J+1) e^{-hcB_0 J(J+1)/kT} .$$

For C_3 the ground state rotational constant $B_0 = 0.43057$ cm^{-1} (Schmuttenmaer et al. 1990). The two parameters T and $N(C_3)$, along with the f-values shown in Table 2, then determine the equivalent width, $W_{J',J''}$, of each transition, using the standard relationship

$$W_{J',J''} = 8.853 \times 10^{-21} \lambda^2 N_J f_{J',J''} , \qquad (2)$$

where $f_{J',J''}$, the oscillator strength for a given transition $J' \leftarrow J''$ at wavelength λ in Å, is given by the product of the electronic oscillator strength f_{ul}, the Franck-Condon factor, and the Hönl-London factor. The units for N_J and

TABLE 2
MOLECULAR DATA FOR THE $A^1\Pi_u \leftarrow X^1\Sigma_g^+$ TRANSITION OF C_3

Wavelength (Å)	Line	$f_{J'J''}$ ($\times 10^3$)[a]
4049.770	$R(24)$	4.24
4049.784	$R(26)$	4.23
4049.784	$R(22)$	4.26
4049.810	$R(20)$	4.30
4049.810	$R(28)$	4.21
4049.861	$R(18)$	4.33
4049.861	$R(30)$	4.20
4049.963	$R(16)$	4.36
4050.081	$R(14)$	4.42
4050.206	$R(12)$	4.48
4050.337	$R(10)$	4.57
4050.495	$R(8)$	4.70
4050.670	$R(6)$	4.92
4050.866	$R(4)$	5.34
4051.069	$R(2)$	6.40
4051.250[b]	$R(0)$	16.00
(4051.309)		
4051.461	$Q(2)$	8.00
4051.519	$Q(4)$	8.00
4051.590	$Q(6)$	8.00
4051.681	$Q(8)$	8.00
4051.741[c]	$P(2)$	1.60
4051.793	$Q(10)$	8.00
4051.929	$Q(12)$	8.00
4052.062	$P(4)$	2.66
4052.089	$Q(14)$	8.00
4052.271	$Q(16)$	8.00
4052.424	$P(6)$	3.08
4052.473	$Q(18)$	8.00
4052.698	$Q(20)$	8.00
4052.792	$P(8)$	3.29
4052.940	$Q(22)$	8.00
4053.180	$P(10)$	3.43
4053.208	$Q(24)$	8.00
4053.490	$Q(26)$	8.00
4053.591	$P(12)$	3.52
4053.794	$Q(28)$	8.00
4054.020	$P(14)$	3.58
4054.112	$Q(30)$	8.00
4054.458	$P(16)$	3.64
4054.908	$P(18)$	3.67
4055.373	$P(20)$	3.70
4055.877	$P(22)$	3.73
4056.410	$P(24)$	3.75
4056.961	$P(26)$	3.77
4057.531	$P(28)$	3.78
4058.121	$P(30)$	3.80

[a] Here $f = 0.0160$ was used, consistent with Maier et al. 2001 and Oka et al. 2003; Roueff et al. 2002 and Galazutdinov et al. 2002 use $f = 0.0146$.

[b] The $R(0)$ assignment by Gausset et al. 1965 (shown parenthetically) is inconsistent with our observations. We use the observed value, confirmed by laboratory measurements (McCall et al. 2003a), in the rotational level population model.

[c] Calculated transition wavelength (Roueff et al. 2002).

W_J are cm^{-2} and Å, respectively. Here we use $f = 0.016$, consistent with Maier et al. (2001) and Oka et al. (2003), for the product f of the electronic oscillator strength and Franck-Condon factor, whereas Roueff et al. (2002) and Galazutdinov et al. (2002) use $f = 0.0146$. Future determinations of the oscillator strength and Franck-Condon factor will scale the derived column densities accordingly. The Hönl-London factors for this band ($\Lambda = 1 \leftarrow 0$) are $(J + 2)/2(2J + 1)$, $1/2$, and $(J - 1)/2(2J + 1)$ for the R-, Q-, and P-branch transitions, respectively. Table 2 shows the adopted wavelengths, assignments, and $f_{J'J''}$ for each transition.

Beginning with an approximate estimate of the C_3 excitation temperature ($T \sim 45$ K), column density [$N(C_3) \sim 10^{12}$ cm^{-2}], and line width (FWHM = 5.2 km s^{-1}), a simulated spectrum was produced. Standard curve-fitting routines were then used to minimize the difference between the observed and simulated spectra, by varying these three parameters [T, $N(C_3)$, and FWHM]. If a second temperature component was observed, in the form of a pronounced R-branch band head that was not reproduced with the single temperature simulation, then a spectrum incorporating two temperatures T_l and T_h and column densities $N_l(C_3)$ and $N_h(C_3)$ was used.

The initial estimate for the line width was larger than the instrument resolution (~4.5 km s^{-1}) and characteristic of the line widths in the observed spectra (Table 3). Broad lines are observed because translucent sight lines typically sample multiple diffuse clouds, which can have velocity separations comparable to, or larger than, our instrumental line width (Welty & Hobbs 2001). The velocity distribution of the clouds, convolved with the instrumental line width, produces observed features that in some cases (e.g., HD 204827) are rather wide. Since we are observing through multiple clouds, the temperatures derived from our model represent an integrated average over all the clouds along the line of sight. In the opposite extreme, the best-fit line widths for X Per and χ Aur are slightly below the instrument profile because of the relatively large level of noise in those spectra.

Figure 1 shows the observed spectra and best-fit thermal excitation model for 10 detections, with model results summarized in Table 3. Measurement uncertainties are discussed in § 3.3.

3.2. *Rotational Level Population Model*

The most common method for determining the population of a particular rotational level J is to measure the equivalent width W of an unblended absorption feature. If multiple transitions ($\Delta J = 0, \pm 1$) from the same lower J state are observed, then each transition probes the same population and multiple measurements of the same quantity may be made.

In the case of our C_3 spectra, the low-J transitions ($J \lesssim 12$) in the R-branch are well resolved, but the stronger Q-branch lines starting from the same J levels pile atop one another. Similarly, transitions from higher J levels that are well resolved in the Q-branch [e.g., $Q(16)$ and $Q(22)$] are blended into a single feature in the R-branch band head. In order to extract information from all of the observed transitions, a model was used that varies the population in each J level as a free parameter, produces a simulated spectrum, and then minimizes the difference between the observed and simulated spectra.

The initial population values for the model were determined from the best-fit thermal distribution. A curve-fitting routine was then used to vary each N_J and minimize the residuals. After fitting the population in each J level, a Boltzmann plot was generated for each source, and kinetic

TABLE 3
BEST-FIT PARAMETERS FOR THERMAL EXCITATION MODEL OF THE OBSERVED SPECTRA

Star	$N(C_3)$[a]	$N_l(C_3)$[a]	$N_h(C_3)$[a]	T_l	T_h	FWHM[b] (km s^{-1})
HD 21483	4.60 ± 0.28	2.60	2.00	28.3 ± 1.3	150 ± 13	5.6 ± 0.1
HD 23180	1.27 ± 0.13	...	...	127.3 ± 3.9	...	5.2 ± 0.2
HD 24398	1.30 ± 0.35	...	...	132 ± 10.3	...	5.1 ± 0.4
HD 24534	1.77 ± 0.19	0.49	1.28	40 ± 6.1	250 ± 41	3.7 ± 1.0
HD 34078	6.21 ± 0.68	...	...	301.4 ± 15.4	...	7.2 ± 0.3
HD 36371	0.75 ± 0.06	0.13	0.62	20.1 ± 2	250 ± 52	3.1 ± 1.2
HD 53367	2.08 ± 0.26	...	...	60.8 ± 1.5	...	5.6 ± 0.1
HD 62542	10.37 ± 0.53	7.35	3.01	75.5 ± 7.2	200 ± 76	5.6 ± 0.1
HD 169454	2.24 ± 0.66	...	...	23.4 ± 1.4	...	6.5 ± 0.4
HD 204827	11.13 ± 0.87	...	...	40.6 ± 0.8	...	8.5 ± 0.2

[a] Column density N in 10^{12} cm^{-2}.
[b] FWHM derived from direct fit to the observed spectrum; instrumental line width at 4050 Å is ~4.5 km s^{-1}.

temperatures that best fit $J \leq 14$ and $J > 14$ were determined. Figure 2 shows the observed and modeled spectra, with Boltzmann plots derived from the fit. The detection limits for each J are shown as dotted lines in the Boltzmann plots. Results from the model are listed in Table 4 with uncertainties discussed below.

3.3. *Uncertainties and Detection Limits*

Uncertainties in the measurement of column densities for individual rotational levels are dependent on the uncertainty in the measurement of the equivalent width W. The 1 σ uncertainty in W is given by

$$\delta W_{1\sigma} = (wd)^{1/2}\sigma \ , \qquad (3)$$

where w is the FWHM of the observed transition (in Å), d is the dispersion of the instrument (in Å pixel^{-1}), and σ is the standard deviation of the normalized continuum—that is, $(S/N)^{-1}$. The δW for each transition is converted to an uncertainty in population, δN_J, using equation (2). For a given J, the transition with the largest oscillator strength will give the smallest uncertainty in N_J. In all cases except the $R(0)$ transition, the Q-branch has the largest oscillator strength for a given J (see Table 2), and this is the f-value we use for our uncertainty estimate.

The detection limits for the total column of C_3 are dependent on the excitation of C_3. A larger total population of C_3 may go undetected if it is distributed among many rotational levels than if the population is all confined to a few low-J rotational levels. For our upper limits listed in Q6 Table 5, we assume that molecules are all distributed evenly among $J = 0$–20. Although the choice of 11 levels among which the distribution is evenly spread is not based on any underlying physics, a comparison to the spectrum of ζ Per shows that for the purposes of estimating our detection limit, such an approach is not unreasonable.

3.4. *The $R(0)$ Transition*

During the initial analysis of the Boltzmann plots, it became evident that $R(0)$ was uniformly underpopulated

TABLE 4
ROTATIONAL LEVEL POPULATIONS DETERMINED BY FITTING THE OBSERVED SPECTRA

	N_J ($\times 10^{11}$ cm^{-2})									
J	HD 21483	HD 23180	HD 24398	HD 24534	HD 34078	HD 36371	HD 53367	HD 62542	HD 169454	HD 204827
0	1.22	0.09	0.34	0.14	0.88	0.15	0.94	2.64	0.49	1.83
2	5.79	0.92	1.01	1.04	2.55	0.27	2.83	6.46	2.13	15.42
4	7.67	1.21	1.54	1.35	3.65	0.42	3.04	10.04	4.66	22.54
6	8.34	1.18	1.69	2.14	4.51	0.42	3.93	12.96	4.73	24.27
8	6.19	1.26	1.84	1.72	7.06	0.21	3.17	15.15	2.27	19.44
10	3.87	1.43	1.61	1.49	7.53	0.29	2.34	11.59	<0.96	11.68
12	2.61	1.29	1.84	1.28	8.03	0.18	2.17	11.04	<0.96	6.53
14	1.43	0.82	1.30	1.36	7.85	<0.15	0.57	9.22	<0.96	4.24
16	1.42	1.19	1.44	1.31	5.30	0.17	0.67	6.94	<0.96	3.48
18	1.90	0.82	1.39	1.26	3.57	0.49	<0.31	5.54	<0.96	<0.76
20	1.26	0.82	0.91	1.10	2.38	0.32	0.51	4.36	<0.96	<0.76
22	0.90	0.73	0.78	0.87	3.65	0.26	<0.31	3.73	<0.96	<0.76
24	1.43	0.82	0.99	0.97	2.74	0.19	<0.31	2.74	<0.96	<0.76
26	0.91	1.13	0.62	0.76	1.83	<0.15	<0.31	1.19	<0.96	<0.76
28	1.14	0.72	0.44	0.91	2.28	<0.15	<0.31	0.73	<0.96	<0.76
30	1.28	0.64	0.52	1.12	1.83	0.44	0.42	0.64	<0.96	<1.15
δN_J[a]	0.40	0.21	0.17	0.27	0.38	0.15	0.31	0.57	0.96	0.76

[a] The 1 σ uncertainty δN_J is determined using eqs. (2) and (3) and $f = 0.016$. Note that δN_J for $R(0)$ is half of the listed value.

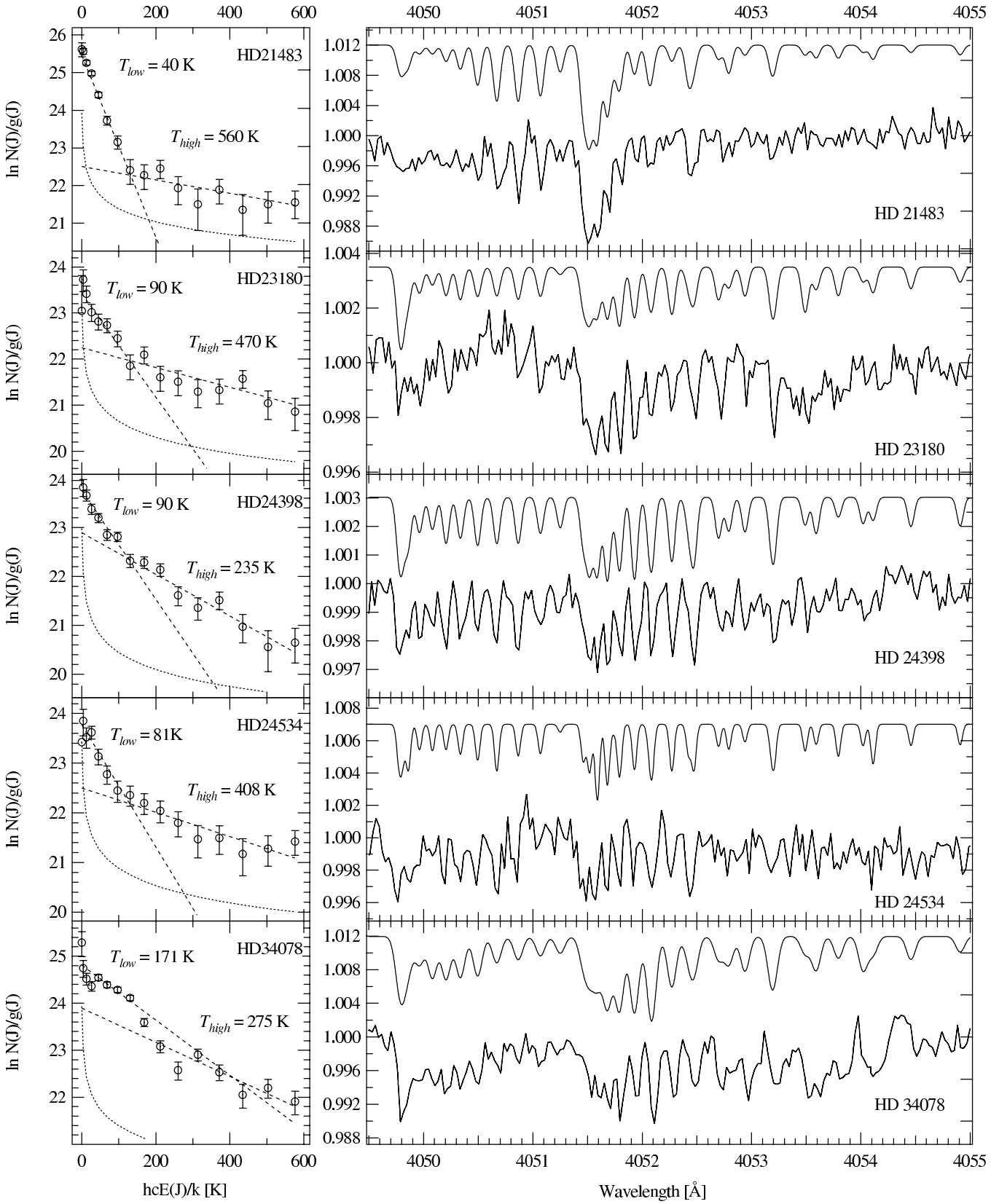

FIG. 2.—Spectra of C_3 detections with rotational excitation model fit (offset for clarity) and the Boltzmann plot (*left*) derived from fit to individual rotational levels. The dotted curve depicts the 1 σ detection limit as a function of J. Points without error bars indicate upper limits. Dashed lines indicate fits to data points for $J \leq 14$ and $J > 14$, where the slope is inversely proportional to kinetic temperature. Note that the spectra are on different intensity scales and the very large columns of C_3 toward HD 62542 and HD 204827.

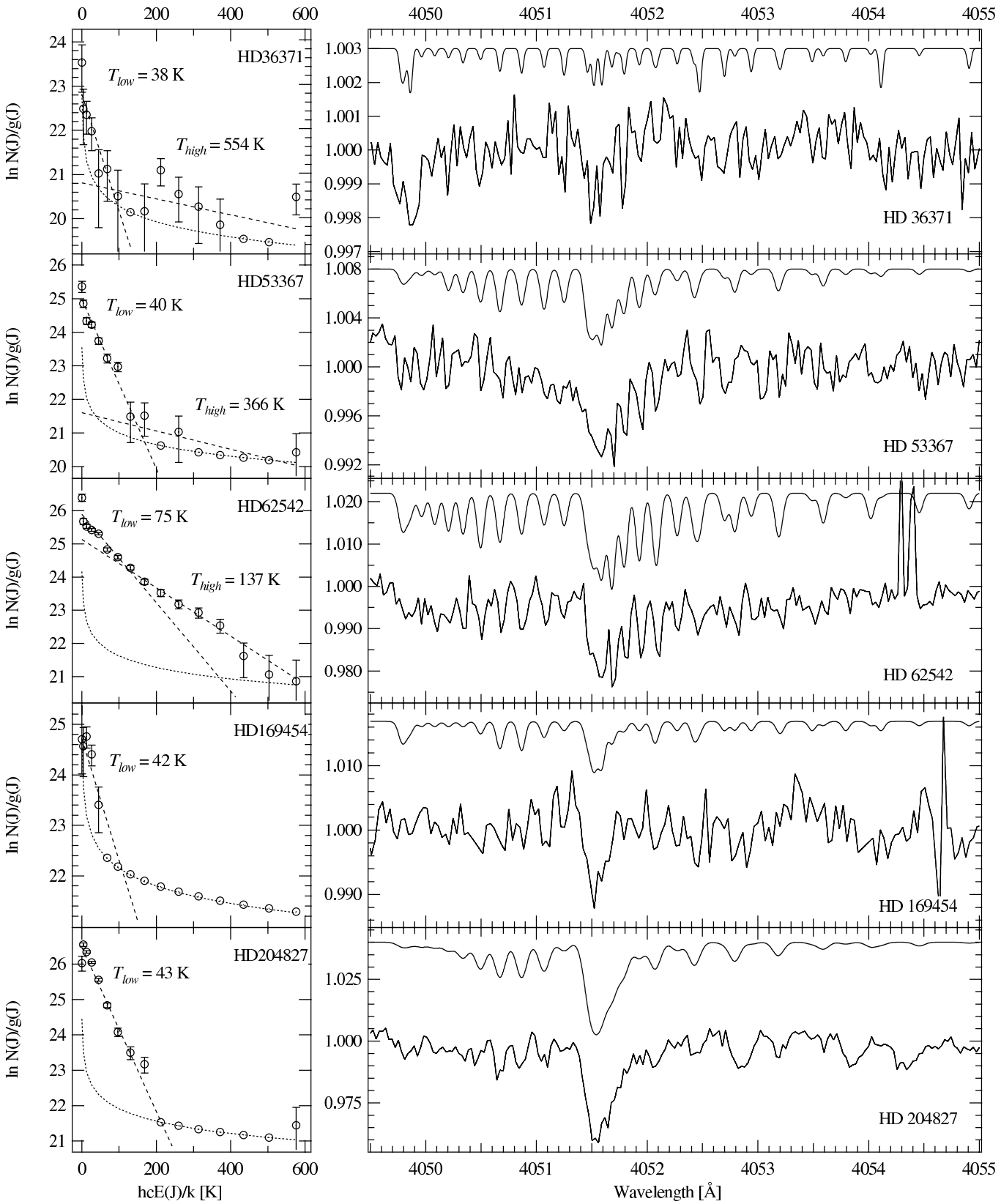

FIG. 2.—*Continued*

relative to what was expected from a thermal distribution that fit $J = 2$–10. A close inspection of the spectra revealed that the observed $R(0)$ transition was significantly shifted toward the blue from the laboratory assignment of Gausset et al. (1965). This was particularly apparent in the spectrum of HD 62542 and can be noted by comparing the thermal excitation model [which uses the Gausset et al. 1965 assignment of $R(0)$] with our observations in Figure 1. Analysis of

TABLE 5
OBSERVED PROPERTIES OF C_3 AND C_2

Star	Name	$N(C_3)$ ($\times 10^{12}$ cm^{-2})	$T_{low}(C_3)$[a] (K)	$T_{high}(C_3)$[b] (K)	$N(C_2)$[c] ($\times 10^{14}$ cm^{-2})	$T(C_2)$[d] (K)	$n_{coll}(C_2)$[d] (cm^{-3})	$N(C_2)/N(C_3)$
HD 21483		4.74 ± 0.28	40	560	1.10 ± 0.30	13 ± 5	190 ± 20	23.2 ± 6.5
		2.2 ± 0.5[e]			0.93[f]			
HD 23180	o Per	1.51 ± 0.13	90	470	0.32 ± 0.12	60 ± 20	200 ± 50	21.2 ± 8.2
		<1.55[e]			0.22 ± 0.03[g]			
HD 24398	ζ Per	1.83 ± 0.35	90	235	0.31 ± 0.08	80 ± 15	460 ± 150	17.0 ± 5.8
		1.0[h]			0.19 ± 0.03[g]			
HD 24534	X Per	1.88 ± 0.19	81	408	0.76 ± 0.20	44 ± 5	225 ± 20	40.4 ± 11.6
		<1.5[e]			0.53[i]			
HD 34078	AE Aur	6.56 ± 0.68	171	275	1.00 ± 0.09	120 ± 10	>500	15.2 ± 2.3
		2.2 ± 0.5[e]			0.58[f]			
HD 36371	χ Aur	0.43 ± 0.06	38	554	0.29 ± 0.11	...	...	68.1 ± 27.9
		<1.29[e]						
HD 53367		2.21 ± 0.26	40	366	0.61 ± 0.16	...	...	27.6 ± 8.1
		<2.2[e]						
HD 62542		10.49 ± 0.53	75	137	0.8 ± 0.2[j]	36 ± 15	510 ± 50	7.6 ± 1.9
HD 148184	χ Oph	2.50 ± 0.43[k,l]			0.43 ± 0.05[g]			17.2 ± 3.6
HD 149757	ζ Oph	1.6[h]			0.25 ± 0.07			16.7 ± 5.5
		1.50 ± 0.29[k,l]			0.24 ± 0.03[g]			
HD 152236		1.8 ± 0.29[k,l]	66	...	0.16 ± 0.06[g]	36 ± 10	300 ± 100	13.3 ± 2.8
HD 169454		2.5 ± 0.66	42	...	1.60 ± 0.29	50 ± 10	>500	64.0 ± 21.8
		4.3 ± 0.5[e]			0.70 ± 0.14[g]			
HD 179406	20 Aql	2.0[h]			0.82 ± 0.15			
		1.3 ± 0.7[e]			0.52[f]			
HD 204827		11.51 ± 0.87	43	...	4.40 ± 0.29	49 ± 5	630 ± 200	38.3 ± 4.1
		10.4 ± 0.5[e]						
HD 210121		3.79[m]			1.00 ± 0.13			
		1.9 ± 0.5[e]			0.65 ± 0.15[n]			

NOTES.—Nondetections of C_3 in this work [with the upper limit $N(C_3)$ in 10^{11} cm^{-2} in parentheses] are as follows: HD 11415 (1.8), HD 20041 (4.2), HD 21398 (3.3), HD 22951 (2.5), HD 24912 (1.6), HD 35149 (2.0), HD 37022 (2.1), HD 37061 (3.3), HD 41117 (1.8), HD 42087 (2.1), HD 43384 (2.6), HD 206267 (3.5), HD 207198 (6.1), and HD 210839 (6.1). Oka et al. 2003 measure C_3 [with $N(C_3)$ in 10^{12} cm^{-2} in parentheses] toward HD 26571 (2.1 ± 0.6), HD 27778 (1.2 ± 0.3), HD 29647 (4.6 ± 1.3), HD 172028 (3.6 ± 0.6), HD 203938 (≤ 1.3), and HD 206267 (2.7 ± 0.4).

[a] Temperature that best fits low ($J \leq 14$) levels of C_3.

[b] Temperature that best fits high ($J > 14$) levels of C_3.

[c] All values from Thorburn et al. 2003 unless otherwise noted and normalized to the oscillator strength $f = 1.0 \times 10^{-3}$.

[d] Temperatures and densities calculated from N_λ values in Table 6.

[e] Oka et al. 2003.

[f] Federman et al. 1994.

[g] van Dishoeck & Black 1986.

[h] Maier et al. 2001.

[i] Federman & Lambert 1988.

[j] Gredel et al. 1993.

[k] Galazutdinov et al. 2002.

[l] Reported equivalent widths have been converted to column densities using oscillator strengths in Table 2 and eq. (2). Weighted averages are used where multiple measurements are reported for the same J and the sum of the N_J is reported here. Note that total $N(C_3)$ reported here is roughly an order of magnitude larger than the values listed in Galazutdinov et al. 2002, which do not include the contributions of all observed rotational levels.

[m] Roueff et al. 2002.

[n] Gredel et al. 1992.

the higher resolution spectra of ζ Oph (Maier et al. 2001) and HD 152236 (Galazutdinov et al. 2002) shows similar indications of a spectral shift; however, neither data set is of sufficient S/N to conclude that there is a significant difference between the observed spectrum and the laboratory assignment. Motivated by this discrepancy, a group including two of us (M. Á. and B. J. M.) revisited the laboratory spectrum of the 4051 Å band of C_3 with higher resolution than our observations (McCall et al. 2003a). Indeed, we found the $R(0)$ transition to be blueshifted from the assignment of Gausset et al. (1965) and consistent with our astronomical spectra. Since $R(0)$ and $P(2)$ share the same upper state, our measurement of the $R(0)$ transition implies that the calculated position of the $P(2)$ line (Table 2) will shift to the blue and overlap $Q(8)$. This is confirmed by laboratory measurements (McCall et al. 2003a).

4. RESULTS AND ANALYSIS

4.1. *Column Density Comparisons*

Table 5 summarizes our measurements of $N(C_3)$, along with previous work. In their determination of C_3 column densities from an extensive, low-resolution survey, Oka et al. (2003) measured the equivalent width of the unresolved Q-branch and assumed that it contained half the total intensity of the C_3 band. While this is a good approximation for a thermal distribution at $T < 50$ K, we note that

this assumption underestimates the total column density when there is significant population in higher J levels. Comparisons of $N(C_3)$ for HD 204827 and HD 169454 show either agreement within error, or a slight overestimate by Oka et al. (2003). Notably, these are the two clouds for which we measure only a low-temperature component in the excitation profile. On the other hand, AE Aur and HD 21483, which show pronounced R-branch band heads (Fig. 2), are underestimated by Oka et al. (2003) because of a significant population of C_3 in high rotational levels.

Our determination of $N(C_3)$ for ζ Per is larger than the measurements of Maier et al. (2001) because of our higher S/N, which allows us to measure the populations in higher J levels. The column density determination for ζ Oph by Roueff et al. (2002), using the data from Maier et al. (2001), is consistent with our measurements and highlights the utility of their model for determining $N(C_3)$.

4.2. *Correlations*

The correlation between C_2 and C_3 pointed out by Oka et al. (2003) may be tested more rigorously with the precise determinations of the C_3 column density presented here. The $N(C_2)$ measurements of Thorburn et al. (2003) are plotted against our measurements of $N(C_3)$ in Figure 3.

The most notable outlier is HD 62542, which has an extremely high column density of C_3, yet an average-to-low column of C_2. The intriguing line of sight toward this star seems to be a highly unorthodox cloud; not only does it seem to be "missing" C_2, it has an extreme UV extinction curve (Cardelli & Savage 1988) and an unusually low column of CH^+ (Cardelli et al. 1990), and it lacks the diffuse bands characteristic of reddened sight lines (Snow et al. 2002). Following the analysis of Cardelli et al. (1990), Snow et al. (2002) have interpreted the lack of DIBs toward this star by suggesting the sight line is dominated by a dense cloud stripped of its diffuse outer layers. Considering the weak DIBs and the seemingly low column of C_2, it is noteworthy that a correlation between C_2 and some DIBs, such as λ4963 and λ5769, has recently been identified (Thorburn et al. 2003). However, the "C_2 DIBs" are in general much weaker than the classical DIBs, such as λ6284 and λ5797, which have been reported to be unusually weak toward HD 62542 (Snow et al. 2002). Nonetheless, one might speculate that the processes that stripped the cloud of its strong DIBs may also have destroyed some of its C_2. On the other hand, it is unclear how C_3 would survive a process that destroys C_2, so one could suggest instead that the conditions in this cloud may favor carbon chain formation. Owing to the peculiarity of the line of sight toward this star, we have excluded it from the correlation analysis.

Fitting all of our targets except HD 62542 shows a correlation between C_2 and C_3 similar to that observed by Oka et al. (2003). The correlation coefficient for this work is 0.898, whereas Oka et al. (2003) report 0.932. HD 169454 appears about 2 σ above the trend line in Figure 3, but the value of $N(C_2)$ reported by Thorburn et al. (2003) is significantly larger than the values reported by van Dishoeck & Black (1989) and Gredel & Münch (1986), which are more consistent with the correlation measured here. AE Aur falls significantly below the trend line; perhaps the same processes that could have destroyed the DIBs and C_2 in HD 62542 have occurred, to a lesser extent, in AE Aur (Snow et al. 2002). Another consideration is the variability with time of the molecular species toward AE Aur, where N(CH) has increased by 20% over the last 10 years (Rollinde et al. 2003). However, there were only 2 years between the observations of C_2 and C_3 reported here, while either $N(C_2)$ is a factor of $\sim$2 below or $N(C_3)$ is a factor of $\sim$2 too large relative to the general trend observed for the other sight lines. The possible enhancement of $N(C_3)$ is significantly larger than expected from the time variability of N(CH) alone.

Since HD 204827 has such a large column of C_3 relative to the rest of the sample, much of the correlation seems to rest on this data point. With the high-sensitivity measurements of $N(C_3)$ presented in this work, the correlation between C_2 and C_3 toward stars with relatively low column

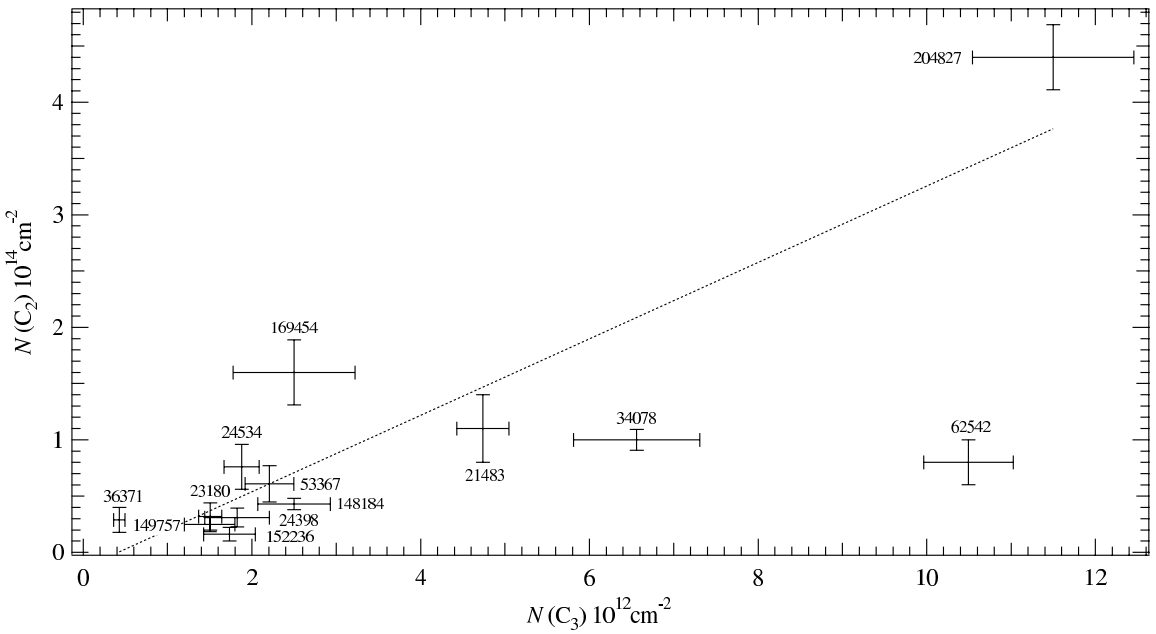

FIG. 3.—Comparison of the column densities of C_3 and C_2; $N(C_3)$ determined in this work is plotted against $N(C_2)$ determinations of Thorburn et al. (2003) along with best fit (*dotted line*). Error bars are 1 σ.

TABLE 6
OBSERVATIONS OF INTERSTELLAR C_2 TOWARD VARIOUS STARS

λ (Å)	LINE	$f_{J'J''}$	W_λ (mÅ)									
			HD 21483[a]	HD 23180[b]	HD 24398[c]	HD 24534[d]	HD 34078[a]	HD 62542[e]	HD 149757[f]	HD 152236[g]	HD 169454[g]	HD 204827[h]
8757.69	R(0)	1.000	9.3 ± 1.2	1.3 ± 0.6	0.57 ± 0.17	1.2 ± 0.2	...	4.4 ± 2	0.7 ± 0.3	0.7 ± 0.5	5.6 ± 1	12.8 ± 5.5
8753.95	R(2)	0.400	5.1 ± 1.6	1.4 ± 0.6	1.06 ± 0.17	1.9 ± 0.5	4.2 ± 1	9 ± 1	1.6 ± 0.3	1 ± 0.5	6 ± 0.5	18.3 ± 2.3
8761.19	Q(2)	0.500	11.5 ± 1.3	1.5 ± 0.6	1.19 ± 0.17	2.8 ± 0.2	3.2 ± 0.7	10 ± 1	1.2 ± 0.3	1.2 ± 0.5	6.6 ± 0.8	23.3 ± 1.8
8766.03	P(2)	0.100	5.6 ± 1.2	...	...	0.5 ± 0.2	...	1 ± 0.5	...	...	1.3 ± 0.3	1.4 ± 3
8751.68	R(4)	0.333	...	...	0.82 ± 0.17	...	3.4 ± 0.9	4.8 ± 1.2	...	...	...	...
8763.75	Q(4)	0.500	7 ± 1.3	1.7 ± 0.6	1.49 ± 0.17	2.9 ± 0.4	5.3 ± 0.6	7.1 ± 2	1.5 ± 0.3	0.9 ± 0.5	7.9 ± 0.7	15.7 ± 2.3
8773.43	P(4)	0.167	...	...	...	...	...	2.6 ± 0.6	...	...	1.7 ± 0.8	...
8750.85	R(6)	0.308	...	1.7 ± 0.6	1.01 ± 0.17	3.2 ± 0.4	...	2.8 ± 1	1.7 ± 0.3	...	...	7.2 ± 2.6
8767.76	Q(6)	0.500	8.1 ± 1.6	1.8 ± 0.6	...	2 ± 0.1	4.6 ± 0.7	1.9 ± 0.9	1.4 ± 0.3	1 ± 0.5	3.9 ± 0.5	14.3 ± 1.1
8782.31	P(6)	0.192	...	...	...	0.1 ± 0.3	...	...	...	...	...	7.3 ± 1.7
8751.49	R(8)	0.294	...	...	0.37 ± 0.17	...	...	...	...	0.4 ± 0.4	...	...
8773.22	Q(8)	0.500	...	0.8 ± 0.6	...	...	...	3.2 ± 0.9	1.9 ± 0.3	...	1.5 ± 0.5	...
8792.65	P(8)	0.206	...	...	...	3 ± 0.2	...	...	...	...	...	...
8753.58	R(10)	0.286	...	...	...	0.7 ± 0.1	...	...	0.4 ± 0.3	...	...	...
8780.14	Q(10)	0.500	...	...	...	...	...	...	...	...	1 ± 0.8	2.2 ± 0.8

[a] Federman et al. 1994;
[b] Hobbs 1981;
[c] Chaffee et al. 1980;
[d] Private communication, Thorburn 2003;
[e] Gredel et al. 1993;
[f] Hobbs & Campbell 1982;
[g] van Dishoeck & Black 1989;
[h] This work.

TABLE 7
ROTATIONAL LEVEL POPULATIONS OF C_2 WITH DERIVED TEMPERATURES AND DENSITIES

	N_J ($\times 10^{14}$)									
J	HD 21483[a]	HD 23180[b]	HD 24398[c]	HD 24534[d]	HD 34078[a]	HD 62542[e]	HD 149757[f]	HD 152236[g]	HD 169454[g]	HD 204827[h]
0	1.4 ± 0.2	0.19 ± 0.09	0.08 ± 0.03	0.17 ± 0.03	...	0.6 ± 0.3	0.1 ± 0.04	0.1 ± 0.07	0.8 ± 0.2	1.89 ± 0.81
2	3.1 ± 0.3	0.47 ± 0.14	0.37 ± 0.04	0.8 ± 0.06	1.1 ± 0.2	2.9 ± 0.2	0.45 ± 0.07	0.36 ± 0.11	2.1 ± 0.1	6.77 ± 0.4
4	2.1 ± 0.4	0.5 ± 0.18	0.42 ± 0.04	0.86 ± 0.1	1.6 ± 0.2	2.2 ± 0.3	0.44 ± 0.09	0.26 ± 0.15	2.3 ± 0.2	4.61 ± 0.7
6	2.4 ± 0.5	0.61 ± 0.15	0.48 ± 0.08	0.61 ± 0.04	1.4 ± 0.2	0.7 ± 0.2	0.52 ± 0.08	0.29 ± 0.15	1.2 ± 0.2	4.24 ± 0.3
8	...	0.24 ± 0.18	0.19 ± 0.09	2.14 ± 0.13	...	0.9 ± 0.3	0.56 ± 0.09	0.1 ± 0.1	0.4 ± 0.2	...
10	...	...	...	0.35 ± 0.08	...	...	0.21 ± 0.15	...	0.3 ± 0.2	0.64 ± 0.2
n_{coll}[i]	190 ± 20	200 ± 50	460 ± 150	225 ± 20	>500	510 ± 50	115 ± 20	300 ± 100	>500	630 ± 200
T[i]	13 ± 5	60 ± 20	80 ± 15	44 ± 5	120 ± 10	36 ± 15	43 ± 20	36 ± 10	50 ± 10	49 ± 5

[a] Federman et al. 1994.
[b] Hobbs 1981.
[c] Chaffee et al. 1980.
[d] J. Thorburn 2003, private communication.
[e] Gredel et al. 1993.
[f] Hobbs & Campbell 1982.
[g] van Dishoeck & Black 1989.
[h] This work.
[i] Estimated systematic uncertainties.

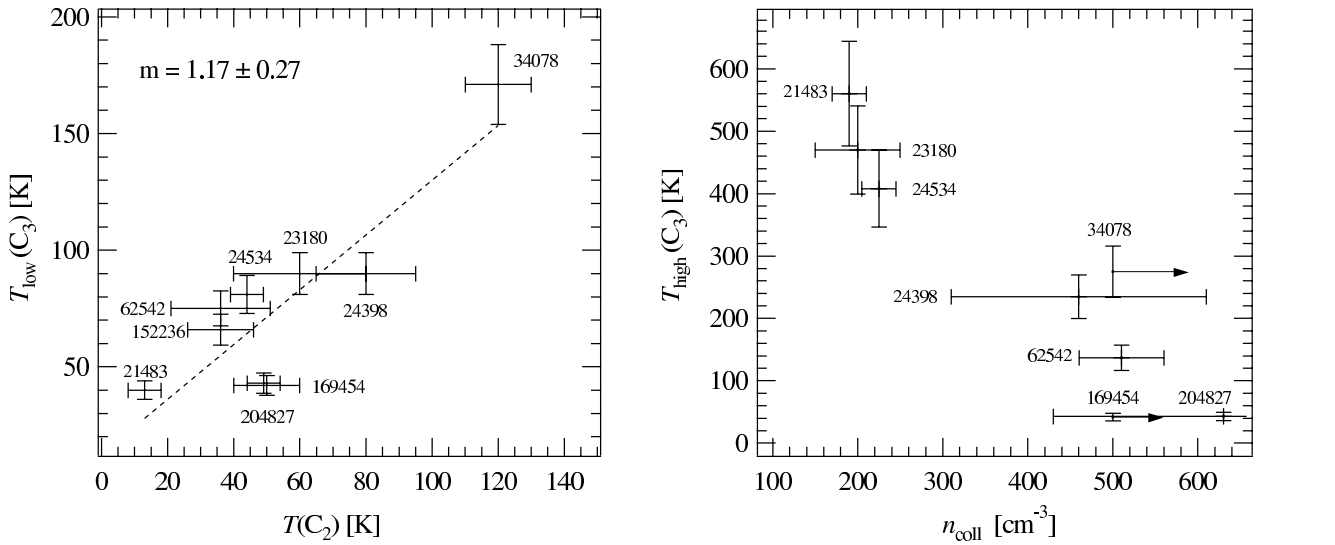

FIG. 4.—Comparison of the excitation of C_3 and C_2. *Left*: Excitation temperatures determined from the observed populations in low ($J \leq 14$) levels of C_3 are compared to the kinetic temperatures determined from the observed excitation of C_2 and the full excitation model of van Dishoeck & Black (1986), showing good agreement. *Right*: Excitation temperature determined from the high ($J > 14$) levels of C_3 is compared with the densities derived from the C_2 excitation model. As expected, T_{high} (C_3) increases with decreasing density.

densities [$N(C_3) < 4 \times 10^{12}$ cm^{-2}] may be tested. Excluding sources with $N(C_3) > 4 \times 10^{12}$ cm^{-2} (i.e., HD 204827, HD 62542, AE Aur, and HD 21483) and HD 169454 for reasons discussed above, we find a correlation coefficient of 0.841, supporting the correlation determined for the entire sample.

The observed correlation between C_2 and C_3 is strikingly similar to the correlation between C_2H and C_3H_2 measured by Lucas & Liszt (2000). In many cases the ratio of $N(C_2)/N(C_3)$ listed in Table 5 falls within the mean abundance ratio $\langle C_2H/o\text{-}C_3H_2 \rangle = 27.7 \pm 8$ measured by Lucas & Liszt (2000). It is unclear if this is coincidence or if there is some underlying chemistry which links these species and their relative abundances.

4.3. *The Excitation of C_2*

The excitation profile of C_3 was compared to the physical conditions determined by the well-understood rotational excitation of C_2. Table 6 summarizes previous observations in the literature of rotationally resolved C_2 toward the stars where we detected C_3. To the existing measurements we have added our C_2 spectrum of HD 204827 measured at Lick and the spectrum of X Per measured at Apache Point Observatory (J. Thorburn 2003, private communication).

All measured equivalent widths were converted to populations using the standard relationship in equation (2). For multiple measurements of the same J level, weighted averages were used for the population. The rotational populations were then simulated using the full C_2 excitation model of van Dishoeck & Black (1982), probing the density-temperature parameter space that determines the excitation of C_2 while minimizing the difference between the model and observed values.[4] In this way a kinetic temperature $T(C_2)$ and a derived density of collision partners, n_{coll}, were deter-
Q7 mined for all targets and are shown in Table 7.

As detailed by van Dishoeck & Black (1982), the derived density n_{coll} is dependent on the collision cross section σ_0 of C_2 with H_2 or H and a scaling factor I for the standard radiation field, which we assume to be 2×10^{-16} cm^2 and 1, respectively. Changes in these values will scale n_{coll} accordingly.

Figure 4 (*left*) shows a comparison of the temperature $T_{low}(C_3)$, determined by fitting the low ($J \leq 14$) rotational levels of C_3, with the kinetic temperature $T(C_2)$ determined from the full-excitation model of C_2. While not unexpected, there is an excellent relationship between the kinetic temperature and the low-J level population of C_3. One would expect the temperature measured by fitting the higher ($J > 14$) rotational levels of C_3 to be inversely related to density, since as the density increases, collisional de-excitation is more efficient at reducing the high rotational level populations. This is indeed observed in the comparison of $T_{high}(C_3)$ versus n_{coll} and is shown in Figure 4 (*right*).

It is interesting to note that the C_3 columns measured toward HD 204827 and HD 169454, which are the two targets that have only low-temperature components (Fig. 2) owing to their high densities ($n_{coll} > 500$ cm^{-3}), are also the targets which deviate most from the trend in the relationship between $T_{low}(C_3)$ and $T(C_2)$. In these high-density targets the kinetic temperature derived from C_2 and the temperature that best fits the excitation of C_3 are the same, whereas the low-density ($n_{coll} < 500$ cm^{-3}) sources all show a somewhat increased excitation temperature of C_3. This is because at high densities the excitation profiles of both C_2 and C_3 are predominantly determined by the kinetic temperature, whereas at low densities the low-J populations, along with the high-lying levels, have a contribution from radiative pumping.

5. SUMMARY

We have observed rotationally resolved spectra of C_3 in 10 translucent sight lines. Using a new method of analysis to accurately retrieve the individual rotational level populations, comparisons have been made with the excitation of C_2, showing excellent agreement in the measurement of

[4] A Web-based C_2 calculator provided by B. J. M. is available at http://dibdata.org/.

kinetic temperature. Trends with density are also consistent with the excitation expected for a nonpolar linear molecule.

With these measurements we have shown that the correlation between $N(C_2)$ and $N(C_3)$, as pointed out by Oka et al. (2003), is maintained for sight lines with a range of $N(C_3)$ from 4.3×10^{11} to 1.2×10^{13} cm^{-2}. The star HD 62542 does not fall on the correlation trend line between $N(C_2)$ and $N(C_3)$ and is shown to have either a very large column of C_3 or depletion in C_2, concomitant with the known weakness of diffuse band features in its spectrum. Similar processes may be occurring to a lesser extent in AE Aur.

Our measurements provide a new challenge for the full C_3 excitation model presented by Roueff et al. (2002), which has been heretofore limited by the quality of observational data.

We thank the referee, J. H. Black, for helpful suggestions that have improved the manuscript. We also wish to acknowledge helpful conversations with L. M. Hobbs, T. Oka, T. P. Snow, J. A. Thorburn, D. E. Welty, and D. G. York. The data presented herein were obtained at the W. M. Keck Observatory and the University of California Observatories/Lick Observatory. The W. M. Keck Observatory is operated as a scientific partnership among the California Institute of Technology, the University of California, and the National Aeronautics and Space Administration and was made possible by the generous financial support of the W. M. Keck Foundation. B. J. M. is supported by the Miller Institute for Basic Research in Science.

REFERENCES

Black, J. H., & Dalgarno, A. 1977, ApJS, 34, 405
Cardelli, J. A., Edgar, R. J., Savage, B. D., & Suntzeff, N. B. 1990, ApJ, 362, 551
Cardelli, J. A., & Savage, B. D. 1988, ApJ, 325, 864
Cernicharo, J., Goicoechea, J. R., & Caux, E. 2000, ApJ, 534, L199
Chaffee, F. H., Lutz, B. L., Black, J. H., van den Bout, P. A., & Snell, R. L. 1980, ApJ, 236, 474
Clegg, R. E. S., & Lambert, D. L. 1982, MNRAS, 201, 723
Douglas, A. E. 1951, ApJ, 114, 466
———. 1977, Nature, 269, 130
Federman, S. R., & Lambert, D. L. 1988, ApJ, 328, 777
Federman, S. R., Strom, C. J., Lambert, D. L., Cardelli, J. A., Smith, V. V., & Joseph, C. L. 1994, ApJ, 424, 772
Galazutdinov, G., Pětlewski, A., Musaev, F., Moutou, C., Curto, G. L., & Krelowski, J. 2002, A&A, 395, 969
Gausset, L., Herzberg, G., Lagerqvist, A., & Rosen, B. 1965, ApJ, 142, 45
Geballe, T. R., McCall, B. J., Hinkle, K. H., & Oka, T. 1999, ApJ, 510, 251
Gredel, R., & Münch, G. 1986, A&A, 154, 336
Gredel, R., van Dishoeck, E. F., & Black, J. H. 1993, A&A, 269, 477
Gredel, R., van Dishoeck, E. F., de Vries, C. P., & Black, J. H. 1992, A&A, 257, 245
Haffner, L. M., & Meyer, D. M. 1995, ApJ, 453, 450
Herbig, G. H. 1995, ARA&A, 33, 19
Hinkle, K. W., Keady, J. J., & Bernath, P. F. 1988, Science, 241, 1319
Hobbs, L. M. 1981, ApJ, 243, 485
Hobbs, L. M., & Campbell, B. 1982, ApJ, 254, 108
Hrivnak, B. J., & Kwok, S. 1999, ApJ, 513, 869
Huggins, W. 1881, R. Soc. London Proc. Ser. I, 33, 1
Jørgensen, U. G. 1994, in IAU Colloq. 146, Molecules in the Stellar Environment, ed. U. G. Jørgensen (Berlin: Springer), 29
Lucas, R., & Liszt, H. S. 2000, A&A, 358, 1069
Maier, J. P., Lakin, N. M., Walker, G. A. H., & Bohlender, D. A. 2001, ApJ, 553, 267
McCall, B. J., Casaes, R. N., Ádámkovics, M., & Saykally, R. J. 2003a, Q8 Chem. Phys. Lett., 374, 583
McCall, B. J., Geballe, T. R., Hinkle, K. H., & Oka, T. 1998, Science, 279, 1910
McCall, B. J., Oka, T., Thorburn, J., Hobbs, L. M., & York, D. G. 2002a, ApJ, 567, L145
McCall, B. J., Thorburn, J., Hobbs, L. M., Oka, T., & York, D. G. 2001, ApJ, 559, L49
McCall, B. J., et al. 2002b, ApJ, 567, 391
———. 2003b, Nature, 422, 500
Oka, T., Thorburn, J. A., McCall, B. J., Friedman, S. D., Hobbs, L. M., Sonnentrucker, P., Welty, D. E., & York, D. G. 2003, ApJ, 582, 823
Raffety, C. W. 1916, Philos. Mag., 32, 546
Rollinde, E., Boissé, P., Federman, S. R., & Pan, K. 2003, A&A, 401, 215
Roueff, E., Felenbok, P., Black, J. H., & Gry, C. 2002, A&A, 384, 629
Rousselot, P., Arpigny, C., Rauer, H., Cochran, A. L., Gredel, R., Cochran, W. D., Manfroid, J., & Fitzsimmons, A. 2001, A&A, 368, 689
Schmuttenmaer, C. A., Cohen, R. C., Pugliano, N., Heath, J. R., Cooksy, A. L., Busarow, K. L., & Saykally, R. J. 1990, Science, 249, 897
Snow, T. P., Seab, C. G., & Joseph, C. L. 1988, ApJ, 335, 185
Snow, T. P., Welty, D. E., Thorburn, J., Hobbs, L. M., McCall, B. J., Sonnentrucker, P., & York, D. G. 2002, ApJ, 573, 670
Thorburn, J. A., et al. 2003, ApJ, 584, 339
van Dishoeck, E. F., & Black, J. H. 1982, ApJ, 258, 533
———. 1986, ApJS, 62, 109
———. 1989, ApJ, 340, 273
Vogt, S. S. 1987, PASP, 99, 1214
Vogt, S. S., et al. 1994, Proc. Soc. Photo-Opt. Instr. Eng., 2198, 362
Welty, D. E., & Hobbs, L. M. 2001, ApJS, 133, 345

Q1 Au: Your article has been edited for grammar, consistency, and to conform to ApJ journal style (see Instructions to Authors). To expedite publication, we generally do not query every routine grammatical and style change made to a manuscript, although all substantive changes have been noted. Please review the article carefully. Note that we may be unable to make changes that conflict with journal style, obscure meaning, or create grammatical or other problems. Also note that article proofs via PDF do not show corrections that will have been made by the typesetter's proofreader, which generally include corrections of errors of page layout, figure placement, and spacing and font mistakes; feel free to mark any errors you notice in these areas. Please also note that it is not ApJ style to have titles on figures. Any text appearing at the top of a figure, with the exception of an axis label, has been removed and incorporated into the legend. **When sending us your corrections, if you are writing them by hand, please print clearly. If sending a fax, please do not write too close to the margins of the page, as these are often cut off in fax transmission. Finally, please note that a delayed, incomplete, or illegible response may delay the publication of your article while we contact you.**

Q2 Au: ApJ follows American usage of "that" to introduce restrictive clauses, "which" for nonrestrictive. Changed "which" to "that," as in "that have been determined..."

Q3 Au: "McCall et al. 2002a" and "2002b" placed in alphabetical order in reference list. Citations have been reversed; please check.

Q4 Au: Table 1: Please provide reference for "Shuping & Snow" or remove citation.

Q5 Au: Table 2: Should "4051.309" (row 17) be merged into the previous row? For example, "4051.250 (4051.309)..."?

Q6 Au: Table 5: Footnote and their references placed in alphabetical order. Please check.

Q7 Au: Table 6 was split into Tables 6 and 7 per our email exchange. Please check carefully.

Q8 Au: Please confirm update of "McCall et al. 2003a.